Coherent and Purcell-Enhanced Emission from Erbium Dopants in a Cryogenic High-Q Resonator

Benjamin Merkel, Alexander Ulanowski, and Andreas Reiserer*

Quantum Networks Group, Max-Planck-Institut für Quantenoptik, Hans-Kopfermann-straße 1, D-85748 Garching, Germany and Munich Center for Quantum Science and Technology (MCQST), Ludwig-Maximilians-Universität München, Fakultät für Physik, Schellingstraße 4, D-80799 München, Germany

(Received 26 June 2020; revised 18 September 2020; accepted 21 September 2020; published 4 November 2020)

The stability and outstanding coherence of dopants and other atomlike defects in tailored host crystals make them a leading platform for the implementation of distributed quantum information processing and sensing in quantum networks. Albeit the required efficient light-matter coupling can be achieved via the integration into nanoscale resonators, in this approach the proximity of interfaces is detrimental to the coherence of even the least-sensitive emitters. Here, we establish an alternative: By integrating a 19 μm thin crystal into a cryogenic Fabry-Perot resonator with a quality factor of 9×10^6, we achieve a two-level Purcell factor of 530(50). In our specific system, erbium-doped yttrium orthosilicate, this leads to a 59(6)-fold enhancement of the emission rate with an out-coupling efficiency of 46(8)%. At the same time, we demonstrate that the emitter properties are not degraded in our approach. We thus observe ensemble-averaged optical coherence up to 0.54(1) ms, which exceeds the 0.19(2) ms lifetime of dopants at the cavity field maximum. While our approach is also applicable to other solid-state quantum emitters, such as color centers in diamond, our system emits at the minimal-loss wavelength of optical fibers and thus enables coherent and efficient nodes for long-distance quantum networks.

DOI: 10.1103/PhysRevX.10.041025 Subject Areas: Quantum Information

The implementation of large-scale quantum networks requires emitters with long ground-state coherence and coherent, spectrally indistinguishable optical transitions [1]. In addition, scaling beyond the demonstrated two-node prototype networks requires highly efficient nodes [2]. In solid-state realizations, achieving these properties simultaneously has proven difficult. Still, recent experiments suggest that this challenge can be overcome by embedding the emitters into an optical resonator [3,4]. This reduces the emission on unwanted transitions and enables a large photon collection probability [5], thus ensuring efficient quantum network nodes. In addition, a large Purcell enhancement factor P leads to spectral broadening that can overcome detrimental effects of spectral instability.

Achieving these benefits requires resonators with large quality factor Q and small mode volume V, as $P \propto Q/V$. The latter has been achieved by confining light in nanophotonic structures [3–8]. Unfortunately, photon-mediated entanglement generation is impaired in nanostructured materials, which typically exhibit increased inhomogeneous broadening and thus spectral mismatch of embedded emitters. In addition, the proximity of interfaces causes a fluctuating charge and spin environment, which leads to reduced coherence and diffusion of the optical transition frequencies [3–8].

Therefore, good optical properties in nanophotonic structures have only been achieved with emitters that are insensitive to electric fields, such as silicon-vacancy centers in diamond [3] or rare-earth dopants in sites with low Stark coefficient [4]. Nanofabrication of suited resonators from these materials requires sophisticated techniques with limited yield and significant loss.

Here, we follow an alternative approach. Instead of using a nanostructured material, we embed a 19 μm thin crystal slab in a cryogenic Fabry-Perot resonator. For ions at the slab center, this increases the distance to the next interface approximately 100-fold. One thus expects that the decoherence induced by surface charge and spin fluctuations is reduced by several orders of magnitude.

To still achieve a high Purcell enhancement, instead of minimizing V we maximize Q by using atomically flat membranes and low-loss dielectric coatings. We thus

*andreas.reiserer@mpq.mpg.de

achieve a quality factor of $Q = 9 \times 10^6$, about 3 orders of magnitude larger than state-of-the-art experiments with emitters in nanophotonic structures [3–8].

While our approach has been pioneered with cold atoms [9], cryogenic Fabry-Perot resonators with lower quality factor have recently been implemented with quantum dots [10], thin diamond membranes [11,12], and rare-earth doped nanoparticles [13,14]. Still, preserving the optical coherence of narrow-band emitters while strongly enhancing their emission via the Purcell effect has not been demonstrated.

To this end, our experiments use erbium dopants in yttrium orthosilicate (YSO), whose transition wavelength around 1536.4 nm ensures minimal loss in optical fibers, as required for quantum networks. Furthermore, the optical coherence of this transition is the best ever measured in a solid, up to 4 ms [15]. While the resulting exceptionally narrow linewidth might offer unique potential for spectrally multiplexed spin-qubit readout [8], it has not been preserved upon integration into nanostructured resonators [7,16]. In contrast, our approach allows for coherence exceeding the lifetime of the strongest-coupled dopants, which is a key enabling step for remote entanglement generation [1].

A sketch of our experimental system is shown in Fig. 1. We use a plano-concave Fabry-Perot resonator with a tunable length around $L = 50$ μm and a mirror radius of curvature $R = 155$ μm, giving a $w_0 = 5.7$ μm waist of the fundamental Gaussian mode. In the cavity, an atomically flat, 19(1) μm thin YSO membrane serves as host for erbium dopants with an estimated concentration <0.3 ppm (see Supplemental Material [17]).

The mirror transmissions of 7(1) and 24(1) ppm for the concave and crystal-covered side are comparable to the absorption and scattering losses, 21(8) ppm, leading to a finesse of $1.2(2) \times 10^5$, a linewidth of 22(2) MHz, and an out-coupling efficiency of $\sim 46(8)\%$ to a single-mode fiber.

Keeping the cavity resonant requires us to control the mirror separation to less than a picometer. Similar to other experiments with lower finesse [12–14], this turned out to be challenging in our closed-cycle cryostat. We therefore combine a vibration isolation platform with fine-tuning via a piezotube. Still, we observe fluctuations of the cavity resonance frequency with a root mean square of 8(2) MHz, comparable to the cavity linewidth, as shown in Fig. 1(c).

To eliminate the residual vibrations via photothermal feedback, we irradiate a laser field at a wavelength of 1564 nm, far detuned from the erbium transition but close to resonance with another longitudinal cavity mode. When the resonator fluctuates, a higher or lower fraction of the laser light is absorbed, which changes the crystal temperature and thus shifts the resonance. Choosing suited parameters, we can thus stabilize the resonator frequency [18].

Before characterizing the effects of this temperature change, we investigate the optical properties of the erbium

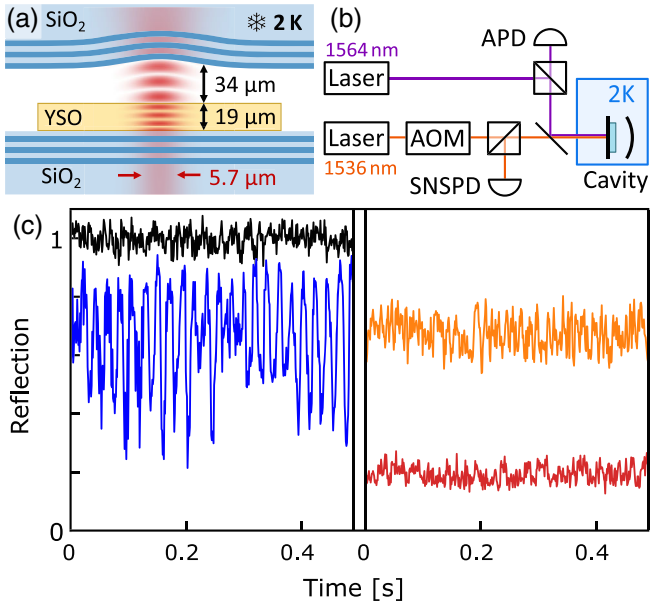

FIG. 1. Experimental setup. (a) Fabry-Perot resonator (not to scale). A stable cavity mode (red) with $\sim 46(8)\%$ out-coupling efficiency toward one side is obtained by embedding a 19(1) μm thin membrane of erbium-doped YSO (orange) between two dielectric mirrors (blue layers of alternating refractive index). (b) Optical setup. The cavity is mounted at 2 K in a closed-cycle cryocooler (blue box). It is probed with a faint laser field, polarized along the $D1$ axis of YSO, and on resonance with the transition of erbium dopants around 1536.4 nm. It is switched by an acousto-optical modulator (AOM) and detected by a superconducting single-photon detector (SNSPD). A second laser field at 1564 nm is detected with an avalanche photodiode (APD). It is resonant with another longitudinal resonator mode and can be used for resonator stabilization. (c) Resonator stability over time. Off-resonant light is fully reflected from the cavity (black). Without active stabilization (left-hand panel), vibrations lead to a fluctuating signal when tuned on resonance (blue). With thermooptical feedback (right), the cavity frequency can be stabilized to the side (orange) or bottom (red) of the reflection.

ensemble by measuring fluorescence after resonant pulsed excitation. At temperatures around 2 K, we apply a magnetic field of 0.8 T along the $D2$ axis of the crystal to ensure that the population is trapped in the probed lower spin state, avoiding detrimental effects of spectral hole burning [19] and superhyperfine couplings [20].

We first investigate the inhomogeneous broadening by sweeping the laser and cavity frequency. In contrast to nanofabricated resonators on the same host [7,8], the observed Lorentzian spectrum with a FWHM of 414(7) MHz (see Supplemental Material [17]) is not broadened compared to bulk reference crystals. This testifies to low strain in our crystalline membrane and indicates that our dopant concentration is low enough to avoid effects of collective strong coupling.

As a next step, we measure the fluorescence at the center of the inhomogeneous distribution. As the dopants are

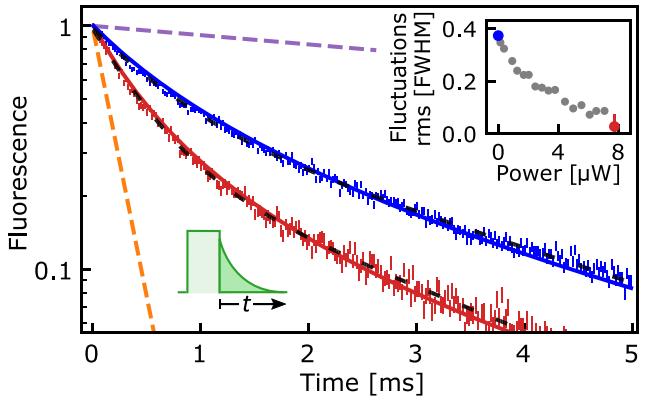

FIG. 2. Purcell-enhanced emission. After pulsed excitation with a power of 54 nW and a duration of 0.5 μs, the fluorescence of resonator-coupled dopants (blue) decays on a faster timescale than in free space (purple dashed line). The decay rate is further enhanced when the cavity is kept on resonance via photothermal feedback (red). In both cases, the decay is well fit by a biexponential curve (black dashed), and in excellent agreement with a numerical modeling of the resonator with no free parameters (red and blue solid curves). According to this model, the decay of dopants at the field maximum (orange dashed line) corresponds to a lifetime-reduction factor of 59(6). The inset shows the fluctuations of the cavity length as a function of feedback laser power, derived by fitting the measured decay to our model.

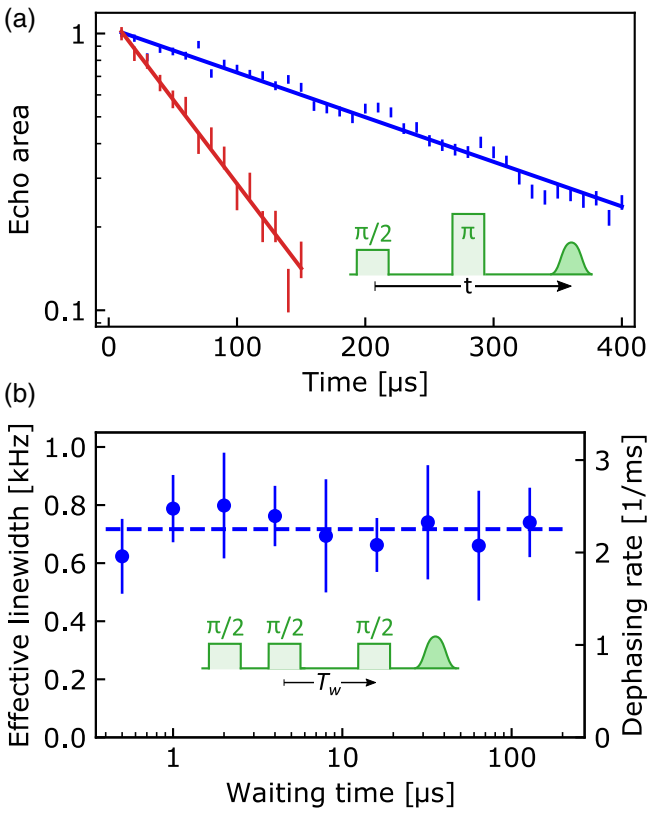

FIG. 3. Optical coherence measurement. (a) Two-pulse photon echo. The used sequence, with 0.5 μs long optical π pulses with a power of 54 nW, is shown in the inset. As expected in the absence of spectral diffusion during the optical lifetime, the coherence decays exponentially with the echo time t. Compared to the situation without photothermal feedback (blue), a faster decay is observed when the resonator frequency is stabilized (red), which we attribute to heating of the crystal. (b) Three-pulse photon echo. We measure the echo after three $\pi/2$ pulses, as shown in the inset. We observe a constant effective linewidth Γ_{eff} independent of the waiting time T_w, which further testifies to the absence of spectral diffusion within the 0.19(2) ms Purcell-enhanced lifetime of the strongest-coupled dopants.

randomly distributed across the Gaussian standing-wave mode of the resonator, the observed signal is an average over many Purcell-enhanced decays with different lifetime. As shown in Fig. 2, our data are well fit by a biexponential decay. A longer lifetime is observed when the cavity is vibrating and thus spends less time on resonance with the dopants.

To gain further insight into the observed decay, we calculate the expected fluorescence using the independently determined cavity properties [21], as detailed in the Supplemental Material [17]. This gives a large Purcell enhancement of $P_{\mathrm{TL}} = 530(50)$ for a two-level system at the maximum of the cavity field. However, the 11% branching ratio of the investigated transition [16], calculated from absorption and lifetime measurements [22], leads to a lower value. For maximally coupled dopants, we thus expect a lifetime reduction by a factor of $P_{\mathrm{Er,max}} + 1 = 59(6)$, which gives $T_1 = 0.19(2)$ ms.

As detailed in the Supplemental Material [17] and shown in Fig. 2, when scaling the calculated Purcell factor with the electric field intensity and averaging over a random dopant distribution in the resonator, the obtained theoretically expected fluorescence curve is in excellent agreement with the data (with no free parameters).

The lifetime is unchanged when the excitation pulse power and thus the number of excited dopants is increased over several orders of magnitude (as shown in the Supplemental Material [17]). We can thus preclude that cavity-enhanced superradiance contributes to the observed lifetime reduction.

We now turn to the optical coherence of the dopants which we study via photon-echo measurements [15,20]. The used pulse sequence is shown as an inset in Fig. 3(a). A first optical pulse with an area of approximately $\pi/2$ prepares an optical coherence that quickly dephases because of the inhomogeneous broadening of our emitters. A second optical π pulse, irradiated after a time $t/2$, leads to a rephasing and thus to the emission of an echo signal at time t. Figure 3(a) shows the measured echo area as a function of t both with (red) and without (blue) photothermal feedback. An exponential fit leads to an optical coherence of $T_2 = 0.14(1)$ ms and $T_2 = 0.54(1)$ ms, respectively.

The observed coherence of the probed ensemble thus exceeds the lifetime of dopants at the field maximum,

$T_2 > T_1$, achieving a key requirement for efficient remote entanglement generation without excessive temporal filtering [9,23].

Remarkably, we even observe a tenfold improvement of the coherence compared to recent measurements with bulk crystals [20], which is explained by the reduction of dopant interactions [19,24] at our lower concentration. In addition, as in both measurements the decay is well fit by a single exponential, we have no indication of homogeneous line broadening via spectral diffusion [25] for maximally Purcell-enhanced dopants.

To confirm this, we performed three-pulse echo measurements, as shown in Fig. 3(b). Here, for several values of the waiting time T_w we determine the effective linewidth by fitting the exponential decay of the echo area when varying the separation between the first two pulses. The observation of a constant effective linewidth up to $T_w = 0.2$ ms indicates that the amplitude or the rate of spectral diffusion in our system is too low to cause decoherence during the lifetime of the best-coupled emitters [26].

In the present configuration, we expect spectral diffusion processes with an effective linewidth of a few hundred kilohertz on longer timescales, presumably seconds, caused by dipolar interactions with the fluctuating nuclear spin bath [25]. Potential detrimental effects can be overcome by a suited choice of the magnetic field direction that gives a zero first-order Zeeman shift, or by regular measurements and compensation of resonance frequency changes [27].

As mentioned, we observe a faster decay of the coherence in the presence of photothermal feedback. We attribute this to the increased temperature. To study this effect, we first confirm that the crystal is thermalized with an adjacent thermometer by comparing the population of the two ground-state spin levels.

We then increase the crystal temperature using a resistive heater. As shown in Fig. 4, the decay rate of the coherence, $1/T_2$, rises with temperature (green), while the lifetime remains unchanged (black). Similarly, the dephasing is increased linearly with the power of the photothermal feedback laser (inset).

At the power required to stabilize the resonator frequency to $1/10$ of its linewidth at the given mechanical fluctuations, $\sim 5\ \mu$W, the dephasing rate is $\sim 5\ \mathrm{ms}^{-1}$. Comparing the curves, we conclude that in this case the crystal temperature is increased by ~ 2 K.

We expect that such temperature increase can be tolerated in other physical platforms that are less affected by thermal decoherence, in particular the NV center in diamond. Here, the demonstrated photothermal feedback can be readily used to suppress the detrimental effects of vibrations that have hampered the use of cryocoolers [12].

In summary, we have shown that integration into high-finesse Fabry-Perot resonators allows for a strong increase of the coupling of dopants to light while preserving their outstanding optical coherence properties.

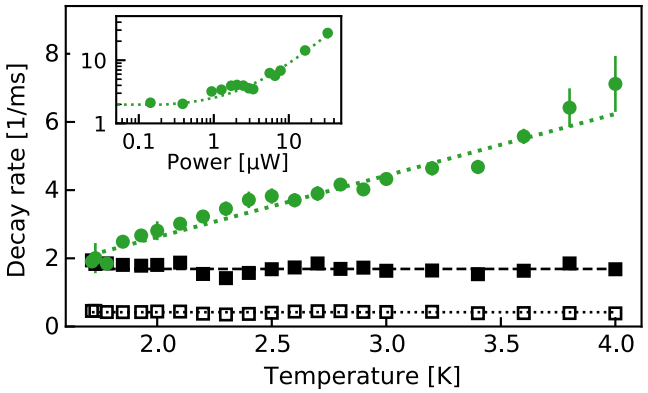

FIG. 4. Temperature dependence. When the temperature of the sample and the exchange gas are increased, the fast (black filled) and slow (black open rectangles) decay constants of the fluorescence remain unchanged (black fit lines). In contrast, the decay rate of the coherence increases (green data and linear fit). The inset shows the rise of the decay rate with increased thermo-optical feedback laser power (green data and linear fit). Based on these measurements, we estimate that at the current vibration level, complete stabilization of the resonator at $\approx 5\ \mu$W (cf. Fig. 2) requires a temperature increase of ~ 2 K.

Our system thus enables efficient, cavity-enhanced quantum memories [28], in which ultralow dopant concentration overcomes the limitations imposed by spin interactions [24]. In addition, the possibly good mode overlap with superconducting resonators facilitates efficient microwave-to-optical conversion [29,30]. Furthermore, spectral hole burning at higher dopant concentration [31] might be used for laser stabilization [32] in the telecom C band for fiber-based sensing or optical atomic clocks.

While the demonstrated possibility to largely decouple the vibrations of a closed-cycle cryocooler may find applications in optomechanical systems [33], it will also give a boost to quantum networking experiments with host crystals that are not amenable to nanofabrication [1]. Using fiber-coupled [10,12–14] or chip-based [34] Fabry-Perot resonators, we still expect that scalable fabrication of quantum network nodes will be feasible.

In our system, the Purcell enhancement can be further increased. First, aligning the polarization along the $D2$ axis of YSO [16] increases the dipole moment twofold compared to our measurements. Second, a tenfold enhancement is expected for mirrors with smaller radius of curvature [9,10,12–14,34]. Finally, the achieved surface quality allows for increasing the finesse by another order of magnitude with better mirror coatings [9,10,34].

Even without these improvements, by operating at the tail of the inhomogeneous broadening [4], we plan to resolve and control single erbium dopants with good optical coherence. Alternatively, host crystals without rare-earth contamination [35–37] or crystals with larger inhomogeneous broadening can be used to this end. Combined with frequency-multiplexed readout of individual spins [8]

and the long ground-state coherence of the ^{167}Er nuclear spin [38], our approach may thus facilitate quantum network nodes operating at ^{4}He temperature and at telecommunication wavelength.

This project received funding from the European Research Council (ERC) under the European Union's Horizon 2020 research and innovation programme (Grant Agreement No. 757772), from the Deutsche Forschungsgemeinschaft (DFG, German Research Foundation) under Germany's Excellence Strategy—EXC-2111—390814868, and from the Daimler-and-Benz-Foundation. We acknowledge the contribution of Natalie Wilson, Manuel Brekenfeld, and Dominik Niemietz in fabricating the concave mirror, and discussions with Alexander Kubanek.

[1] D. D. Awschalom, R. Hanson, J. Wrachtrup, and B. B. Zhou, *Quantum Technologies with Optically Interfaced Solid-State Spins.*, Nat. Photonics **12**, 516 (2018).
[2] S. Wehner, D. Elkouss, and R. Hanson, *Quantum Internet: A Vision for the Road Ahead*, Science **362**, 303 (2018).
[3] A. Sipahigil *et al.*, *An Integrated Diamond Nanophotonics Platform for Quantum-Optical Networks*, Science **354**, 847 (2016).
[4] J. M. Kindem, A. Ruskuc, J. G. Bartholomew, J. Rochman, Y. Q. Huan, and A. Faraon, *Control and Single-Shot Readout of an Ion Embedded in a Nanophotonic Cavity*, Nature (London) **580**, 201 (2020).
[5] P. Lodahl, S. Mahmoodian, and S. Stobbe, *Interfacing Single Photons and Single Quantum Dots with Photonic Nanostructures*, Rev. Mod. Phys. **87**, 347 (2015).
[6] A. Faraon, P. E. Barclay, C. Santori, K.-M. C. Fu, and R. G. Beausoleil, *Resonant Enhancement of the Zero-Phonon Emission from a Colour Centre in a Diamond Cavity*, Nat. Photonics **5**, 301 (2011).
[7] A. M. Dibos, M. Raha, C. M. Phenicie, and J. D. Thompson, *Atomic Source of Single Photons in the Telecom Band*, Phys. Rev. Lett. **120**, 243601 (2018).
[8] S. Chen, M. Raha, C. Phenicie, S. Ourari, and J. Thompson, *Parallel Single-Shot Measurement and Coherent Control of Solid-State Spins below the Diffraction Limit*, arXiv:2006.01823.
[9] A. Reiserer and G. Rempe, *Cavity-Based Quantum Networks with Single Atoms and Optical Photons*, Rev. Mod. Phys. **87**, 1379 (2015).
[10] D. Najer *et al.*, *A Gated Quantum Dot Strongly Coupled to an Optical Microcavity*, Nature (London) **575**, 622 (2019).
[11] D. Riedel, I. Söllner, B. J. Shields, S. Starosielec, P. Appel, E. Neu, P. Maletinsky, and R. J. Warburton, *Deterministic Enhancement of Coherent Photon Generation from a Nitrogen-Vacancy Center in Ultrapure Diamond*, Phys. Rev. X **7**, 031040 (2017).
[12] S. Bogdanović *et al.*, *Design and Low-Temperature Characterization of a Tunable Microcavity for Diamond-Based Quantum Networks*, Appl. Phys. Lett. **110**, 171103 (2017).
[13] B. Casabone, J. Benedikter, T. Hümmer, F. Oehl, K. de Oliveira Lima, T. W. Hänsch, A. Ferrier, P. Goldner, H. de Riedmatten, and D. Hunger, *Cavity-Enhanced Spectroscopy of a Few-Ion Ensemble in* $Eu^{3+}:Y_2O_3$, New J. Phys. **20**, 095006 (2018).
[14] B. Casabone *et al.*, *Dynamic Control of Purcell Enhanced Emission of Erbium Ions in Nanoparticles*, arXiv:2001.08532.
[15] T. Böttger, C. W. Thiel, R. L. Cone, and Y. Sun, *Effects of Magnetic Field Orientation on Optical Decoherence in* $Er^{3+}:Y_2SiO_5$, Phys. Rev. B **79**, 115104 (2009).
[16] E. Miyazono, T. Zhong, I. Craiciu, J. M. Kindem, and A. Faraon, *Coupling of Erbium Dopants to Yttrium Orthosilicate Photonic Crystal Cavities for On-Chip Optical Quantum Memories*, Appl. Phys. Lett. **108**, 011111 (2016).
[17] See Supplemental Material at http://link.aps.org/supplemental/10.1103/PhysRevX.10.041025 for details on the experimental setup, the cavity properties, and the theoretical modeling.
[18] J. F. S. Brachmann, H. Kaupp, T. W. Hänsch, and D. Hunger, *Photothermal Effects in Ultra-Precisely Stabilized Tunable Microcavities*, Opt. Express **24**, 21205 (2016).
[19] B. Car, L. Veissier, A. Louchet-Chauvet, J.-L. Le Gouët, and T. Chanelière, *Optical Study of the Anisotropic Erbium Spin Flip-Flop Dynamics*, Phys. Rev. B **100**, 165107 (2019).
[20] B. Car, J.-L. Le Gouët, and T. Chanelière, *Superhyperfine Induced Photon-Echo Collapse of Erbium in* Y_2SiO_5, Phys. Rev. B **102**, 115119 (2020).
[21] E. Janitz, M. Ruf, M. Dimock, A. Bourassa, J. Sankey, and L. Childress, *Fabry-Perot Microcavity for Diamond-Based Photonics*, Phys. Rev. A **92**, 043844 (2015).
[22] T. Böttger, Y. Sun, C. W. Thiel, and R. L. Cone, *Spectroscopy and Dynamics of* $Er^{3+}:Y_2SiO_5$ *at* 1.5 μm, Phys. Rev. B **74**, 075107 (2006).
[23] C. Nölleke, A. Neuzner, A. Reiserer, C. Hahn, G. Rempe, and S. Ritter, *Efficient Teleportation between Remote Single-Atom Quantum Memories*, Phys. Rev. Lett. **110**, 140403 (2013).
[24] B. Merkel, P. Cova Fariña, N. Herrera Valencia, and A. Reiserer, *Dynamical Decoupling of Interacting Anisotropic Spin Ensembles*, arXiv:2005.08822.
[25] T. Böttger, C. W. Thiel, Y. Sun, and R. L. Cone, *Optical Decoherence and Spectral Diffusion at* 1.5 μm *in* $Er^{3+}:Y_2SiO_5$ *versus Magnetic Field, Temperature, and* Er^{3+} *Concentration*, Phys. Rev. B **73**, 075101 (2006).
[26] *Spectroscopic Properties of Rare Earths in Optical Materials*, Springer Series in Materials Science, edited by G. Liu and B. Jacquier (Springer-Verlag, Berlin, 2005).
[27] L. Robledo, H. Bernien, I. van Weperen, and R. Hanson, *Control and Coherence of the Optical Transition of Single Nitrogen Vacancy Centers in Diamond*, Phys. Rev. Lett. **105**, 177403 (2010).
[28] M. Afzelius, N. Gisin, and H. de Riedmatten, *Quantum Memory for Photons*, Phys. Today **68**, No. 12, 42 (2015).
[29] L. A. Williamson, Y.-H. Chen, and J. J. Longdell, *Magneto-Optic Modulator with Unit Quantum Efficiency*, Phys. Rev. Lett. **113**, 203601 (2014).
[30] Y.-H. Chen, X. Fernandez-Gonzalvo, and J. J. Longdell, *Coupling Erbium Spins to a Three-Dimensional*

Superconducting Cavity at Zero Magnetic Field, Phys. Rev. B **94**, 075117 (2016).

[31] D. O. Krimer, B. Hartl, and S. Rotter, *Hybrid Quantum Systems with Collectively Coupled Spin States: Suppression of Decoherence through Spectral Hole Burning*, Phys. Rev. Lett. **115**, 033601 (2015).

[32] S. Cook, T. Rosenband, and D. R. Leibrandt, *Laser-Frequency Stabilization Based on Steady-State Spectral-Hole Burning in* $Eu^{3+}:Y_2SiO_5$, Phys. Rev. Lett. **114**, 253902 (2015).

[33] M. Aspelmeyer, T. J. Kippenberg, and F. Marquardt, *Cavity Optomechanics*, Rev. Mod. Phys. **86**, 1391 (2014).

[34] G. Wachter *et al.*, *Silicon Microcavity Arrays with Open Access and a Finesse of Half a Million*, Light Sci. Appl. **8**, 37 (2019).

[35] S. Bertaina, S. Gambarelli, A. Tkachuk, I. N. Kurkin, B. Malkin, A. Stepanov, and B. Barbara, *Rare-Earth Solid-State Qubits*, Nat. Nanotechnol. **2**, 39 (2007).

[36] C. M. Phenicie, P. Stevenson, S. Welinski, B. C. Rose, A. T. Asfaw, R. J. Cava, S. A. Lyon, N. P. de Leon, and J. D. Thompson, *Narrow Optical Line Widths in Erbium Implanted in* TiO_2, Nano Lett. **19**, 8928 (2019).

[37] L. Weiss, A. Gritsch, B. Merkel, and A. Reiserer, *Erbium Dopants in Silicon Nanophotonic Waveguides*, arXiv:2005.01775.

[38] M. Rančić, M. P. Hedges, R. L. Ahlefeldt, and M. J. Sellars, *Coherence Time of over a Second in a Telecom-Compatible Quantum Memory Storage Material*, Nat. Phys. **14**, 50 (2018).